Fault Location Approach for UPFC based Line Integration Employing Sparse S-Transform

Mohan P. Thakre[1], Nikhil N. Ahire[2], Dinesh M. Chaudhari[3], Rajesh D. Bhirud[4], Ravina G. Ade[5]

[1-5]Dept. of Electrical Engineering, K.K.W.I.E.E.R. Nashik, MH-India
[1]mohanthakre@gmail.com, [2]nikhilahire5555@gmail.com, [3]dsmchaudhari@gmail.com,[4]rajbhirud13@gmail.com, [5]ravinaade23@gmail.com

Abstract: Incorporation of FACTs controller in transmission lines adversely affects the functioning of distance relaying and hinders the accurateness of a zone of transmission lines that is not permissible. This article represents a unique strategy for locating faults across the UPFC-based transmission system. The fault-finding approach is based on a sparse S-transform (SST). The SST has a computationally high altitude comparison to the initial discreet ST, as it uses selective signal frequency bands and therefore is suitable for various relay application domains. Several faults have been identified, such as including and excluding the UPFC in the computational performance assessment.

1. Introduction

Power systems are seeing a bring excellent in transmission networks, with an unceasing availability besides power in the past years. It's often beneficial to operate power transmission nearest to their thermal as well as stability constraints. As a consequence, various sorts of FACTS controllers are being used in the network to eliminate transmission line constraints [1]. Rapid and precise detection and diagnosis of faults play an important part in maintaining the accuracy and stability of the system. Long transmission networks have been protected by distance protection, which is premised on the evaluation of apparent impedance by the use of current as well as voltage, which is observed at relay installation position. Integration of FACT controllers into the system creates issues in the line protection scheme even though they alter the system voltages and currents in a steady-state also in a transient state, according to the operation condition. UPFC (United Power Flow Controller) is indeed a consolidated STATCOM-SSSC controller for multi-application of power systems [1-10].

A detailed literature survey of involvement of the UPFC over distance relay for various parameters, such as the operating mode impact of a controller, inception angle, fault resistance, coupling point, system conditions such as power swings, and protection control parameters have been suggested [2-8]. When UPFC exists within the fault circuit, the voltages and the protective relay streams are changed. Besides, deviations were caused in the assessment of apparent protective impedances and malfunctioning. Fault locating such a system is a critical job and it should be accurate and robust to use the protection scheme. It is studied in [9] that a TCSC is integrated into the transmission system and its influence on the mho remote relay. The implementation of the HVDC bipolar distance relay system is described in [10]. The Wavelet-based digital remote security technique network has been described [11, 12] as well as the methods were therefore reviewed over several faults in such a variety of environments.

The combined method of classification of faults for transmission line has been proposed in [13] besides Wavelet and fuzzy logic and for fault classification, under various system circumstances, the fuzzy logic classifier has been used. While DWT is best (for its ease of use), in some cases it loses its reliability. The presence of noise in the signal, DC, and sub-harmonic elements is thus a risk that the approach will be accurate. The S-transform [14] is an adaptable time-frequency transformation, also known as a wavelet extending that has to use a shifting and extensible Gaussian window. Therefore, the time-domain-signal can be better frequency-dependent, even in the presence of noise non-state resolution. The series compensated transmission system and the ST pattern-recognition approach is simulated in [15] used as a TCSC and fixed condenser. In mitigating distance relaying problems caused by the SVC, a synchro-phasor-measured technique was implemented [16].In [17] the system

failures to locate faults of the multi-terminal structure have shown a technique based on the time of arrival of transitory waves. Although conventional ST has a good MRA attribute, it suffers however from certain minuses such as higher calculations, which can result in protective delays. In [18] a quick version of S-transform was presented and applied to the transmission model cross differential scheme protection, including a STATCOM. To identify, classify and locate system defects, the Sparse ST approach for the remote protection of FACTs Controller [19, 20] illustrated.

In [21], the system defects using the UPFC wind farms have been identified and classified by a distance protection algorithm, based on sign computation of the end of lines and S-matrix CUMSUM. In [22], a control scheme for series FACTs to mitigate the oscillations caused by SSR has been suggested. An application of a FACTs controller for sub-synchronous resonance mitigation could be seen in [23]. Paper Corporation, Section 1, introduces, Section 2, presents sparse ST expression in matrix form, Fault Impedance and location calculations of Section 3. The results of the simulation including impedance pathways for faults with and without the UPFC are explained in Section 4. Signals from different that fault location assessments are finished in Section 5.

2. Sparse S-Transformation

A matrix design [19] of an S-transform by using FFT is shown below. An array of signal samples which may be current or voltage Xi $(i=1, 2, 3... N)$, shall be considered as below to obtain DFT.

$$X = DFT(x_i, i = 1 : N) \tag{1}$$

And the components were also,

$$X_n = \sum_{i=1}^{N} x_i\, e^{(-2\pi j(n-1)(i-1))}, j = \sqrt{-1} \tag{2}$$

The inverse DFT shall be made available as,

$$x_n = \left(\frac{1}{N}\right)\sum_{i=1}^{N} a_i e^{(2\pi i(n-1)(i-1))} \tag{3}$$

Below, the power of N ought to be chosen as 2 to enable the algorithm in the DSP. For window localization which includes the number of frequency elements in frequency as well as time, a Gaussian matrix $C_{M\times N}$ is obtained (10), Value of the frequency m is chosen depending upon the type of scaling. Besides, matrix G has been determined by-product of matrix Y and matrix C as [17],

$$G_{(m,n)} = Y_{(m,n)} \times C_{(m,n)} \tag{4}$$

Matrix G contains signal characteristics in both the domain such as frequency as well as time domain. The SST is obtained by computing the inverse DFT of all the rows localized in time which signifies a definite frequency sinusoid as shown below,

$$SST_{M\times N} = IDFT(G_{M\times N}) \tag{5}$$

Though each component of a transform *tf (f, t)* throughout the $SST_{(m, n)}$ has been acquired as,

$$SST_{(m,n)} = \left(\frac{2}{N}\right)\sum_{i=1}^{N} G_{(m,i)} \exp\left(\frac{2\pi j(n-1)(i-1)}{N}\right) \tag{6}$$

An SST matrix contains instantaneous phasor (IP) variables for indivisible frequency. The fast SST method is possible if the appropriate frequency scaling is chosen. Harmonic scaling is adopted in this study for ease of computing and simplicity.

Inharmonic scaling, the frequency samples selected to have only fundamental and harmonic frequency components, and the other frequencies are excluded for fault analysis. Once frequency scaling is done, estimation of matrix *C*, *G*, *Y*, and *SST* turn out to be faster than the S-transform. Also, by using zeroes,

the sparsity is formed throughout the rows of an SST matrix and the components of the G matrix get to be,

$$G_{(m,n)} = \begin{cases} Y_{(m,n)} \times C_{(m,n)} & if\ (m \in \rho f) \\ 0 & otherwise \end{cases} \tag{7}$$

$$SST_{(m,n)} = \begin{cases} \left(\frac{2}{N} \sum_{i=1}^{N} G_{(m,i)} \exp\left(\frac{2\pi j(n-1)(i-1)}{N} \right) \right) & if\ (m \in \rho f) \\ 0 & otherwise \end{cases} \tag{8}$$

Independent of high-frequency components, this same are obtained from matrices. As well as the instantaneous phasor of the Mth harmonic component could be acquired using M^{th} row of *C, Y, G,* & *SST* matrices. Thus, the expressions of the matrices become more like,

$$Y_{M \times N} = \begin{bmatrix} y_{M+1} & y_{M+3} \cdots & y_{M-1} & y_M \end{bmatrix} \tag{9}$$

$$C_{M \times N} = \begin{bmatrix} c(f_M, t_1) \cdots & c(f_M, t_n) \cdots & c(f_M, t_N) \end{bmatrix} \tag{10}$$

$$G_{M \times N} = \begin{bmatrix} g(f_M, t_1) \cdots & g(f_M, t_n) \cdots & g(f_M, t_N) \end{bmatrix} \tag{11}$$

$$SST_{M \times N} = \begin{bmatrix} tf(f_M, t_1) \cdots & tf(f_M, t_n) \cdots & tf(f_M, t_N) \end{bmatrix} \tag{12}$$

Inharmonic scaling the additions of $N(N-1)(1-K_H)$ and $N(N+K_H(N+2))$ and multiplications are comprised [17]. Here, K_H indicates odd-harmonic frequencies and $K_H \ll (N/2)$. Since K_H and K_A have become lesser than ($N/2$), the difficulty of evaluating SST methodologies has been lower in comparison to the normal S-transform technique.

Original S-transform takes 0.0580 seconds for processing 10 cycles of data (640 samples), while Sparse ST employing Harmonic scaling takes less time 0.0048 seconds, using a 2.4 GHz CPU signal processor. Since beyond the seventh the magnitude of harmonics is minute, frequency points are reduced from 1920 Hz to 350 Hz which results in a considerable increase in the computation speed for the harmonic scaling SST. Further, the fundamental frequency may therefore contain small deviations, while the scaling analysis contains ±2 Hz frequency samples of the basic as well as relating harmonic components.

The *V* or *I* signal *x(k)* is such a discreet process of making decisions be conveyed when

$$X_{1 \times K} = \begin{bmatrix} x_1 & x_2 \cdots & x_K \cdots & x_{(K-1)} & x_k \end{bmatrix} \tag{13}$$

Where, *K* is the total samples which range is $k = K_I \times N_s$, $K_I > 0$. The Sparse ST of the above *V* or *I* samples shall be provided as,

$$\left[SST_i \right]_{M \times N} = SST\left(\begin{bmatrix} x_{(i+1)}, & x_{(i+2)}, & x_{(i+3)} \cdots & x_{(i+N_s-1)}, & x_{(i+N_s)} \end{bmatrix} \right) \tag{14}$$

Where, $i = 0, N_S, 2N_S, 3N_S, \dots, (l-2)N_S, (l-1)N_S$.

The real-time magnitude, as well as phase of the signal generated by the SST-matrix, is shown below.

$$\left[A_i \right]_{M \times N} = \sqrt{real\left(\left[SST_i \right]_{M \times N} \right) + imag\left(\left[SST_i \right]_{M \times N} \right)^2} \tag{15}$$

By using a phase correction, the accurate phase of the signal in radians has been achieved

$$\varphi_{true} = \varphi_{FFST} - 2\pi\left(\frac{f}{f_s}\right) \quad \dots \text{(Radian)} \tag{16}$$

Where, f_s – Sampling frequency (Hz) and f – Signal frequency (Hz) In Eqn. (15) the Mth & N^{th}, which are rows and columns associated with the N point of time as well as the M point of frequency. Thus, for each moment as well as frequency point combination, this same instantaneous phasor of the signals has been acquired at that specific frequency.

3. Analysis of Fault Point Impedance

3.1. Case 1: Fault before UPFC

Figure1 illustrates the schematic of the study system. The UPFC is installed between E-F of the transmission line. A voltage source V_{se} in series and current source I_{sh} in shunt with the line represents the UPFC. For section A1–E of the line, fault loop model for the fault before UPFC is obtained as,

$$V_{A1} = \left(d_{L1}\times(Z_{L1}\times I_1)\right) - (R_{F1}\times I_F) = 0 \tag{17}$$

d_{L1} – unknown fault distance found by resolving (21) into real and imaginary parts as,

$$Re(V_{A1}) - d_{L1}\times Re(Z_{L1}\times I_1) - R_{F1}Re(I_F) = 0 \tag{18}$$

$$Im(V_{A1}) - d_{L1}\times Im(Z_{L1}\times I_1) - R_{F1}Im(I_F) = 0 \tag{19}$$

$$I_F = I_1 + I_3 + I_{sh} \tag{20}$$

Eqn. (20) signifies the summation of the observed currents at Bus $A_1(I_1)$, STATCOM (Ish) and bus$B_1(I_3)$. On section A1-E, d_{L1}- fault distance to be calculated, measured up to fault C from bus-, R_{F1} - unknown R_F and the V_{A1} and I_1 – fault circuit V & I. The Z_{L1} is the impedance for section A1-E of the line respectively. The unknown fault distance is estimated by eliminatingR_{F1},

$$d_{L1} = \frac{(Re(V_{A1})\times Im(I_F)) - (Im(V_{A1})\times Re(I_F))}{(Re(Z_{L1}\times I_1)\times Im(I_F)) - (Im(Z_{L1}\times I_1)\times Re(I_F))} \tag{21}$$

By adding d_{L1} in (17), we can find the unknown resistance,

$$R_{F1} = \frac{(Re(V_{A1}) - (d_{L1}\times Re(Z_{L1}\times I_1)))}{Re(I_F)} \tag{22}$$

The presented scheme design is based on the SONET architecture assumption which follows redundant asymmetric communication and causes end-to-end time delay (few ms).
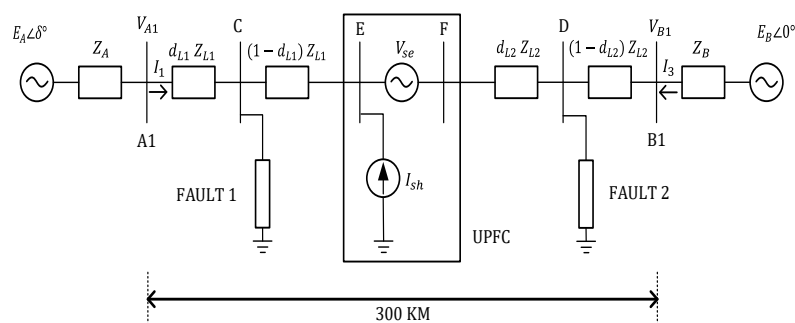

Figure 1. 500kV transmission line included with a UPFC

3.2. Case 2: Fault after UPFC

This algorithm takes into consideration of the shunt capacitance effect of the lumped parameter system throughout order to send $V_{AN}(i)$ & $I_1(i)$ from terminal A1 to E. Each sequence of the current and voltage signals observed from A1 to E is transmitted.

Transferring voltage $V_{A1}(i)$ from A1 to E, the equations are obtained as follows,

$$V_E(i) = cosh(g_{L1}(i)L_{L1}) \times V_{A1}(i) - Z_{sL1}(i)sinh(g_{L1}(i)L_{L1}) \times I_1(i)$$

(23)

Where, L_{L1} - length of line section A1-E in km, $Y_{L1}^P(i)$ -shunt admittance of section AI-E for i^{th} sequence (Ω/km), $Z_{L1}^P(i)$ - series impedance of section A1-E for i^{th} sequence (Ω/km), $Z_{sL1}(i) = \sqrt{\frac{Z^p_{L1}(i)}{Y^p_{L1}(i)}}$ - surge impedance of the line section A1-E for i^{th} sequence and $\gamma_{L1} = \sqrt{Z_{L1}^p(i)Y_{L1}^p(i)}$ - propagation constant of the section A1-E for i^{th} sequence. Also, transferred current I_1 from the segment A1-E yields to below Eqn.

$$I_4(i) = \frac{-\sinh(\gamma_{L1}(i)L_{L1})}{Z_{SL1}(i)} \times V_{A1}(i) + \cosh(\gamma_{L1}(i)L_{L1}) \times I_1(i)$$

(24)

The current flowing from E point to D point has been acquired in the faulty segment E-B1,

$$I_E = I_4 + I_{sh}$$

(25)

For the fault placement algorithm, this same fault loop current and voltage have been analysed, and the fault loop formula could be formulated after UPFC.

$$V_E = a_1V_E(1) + a_2V_E(2) + a_oV_E(0)a$$

(26)

$$I_E = a_1I_E(1) + a_2I_E(2) + \frac{Z_{L1}(0)}{Z_{L2}(1)}a_0I_E(0)$$

(27)

Where, weighting coefficients are a_1, a_2, and a_3 from the symmetrical component analysis.

$$V_{se} = a_1V_{se}(1) + a_2V_{se}(2) + a_0V_{se}(0)$$

(28)

The fault loop equation is obtained as,

$$V_E - V_{se} - ((1 - d_{L2}) \times Z_{L2}(1)) \times I_E - (R_{F2} \times I_F) = 0$$

(29)

Where, d_{L2} is specified as Fault distance on section E-B1 (to be calculated), R_{F2} is the unknown fault resistance, V_E & I_E voltage and current in the faulted loop, Z_{L2} (1) is + Sequence impedance of section E-B1.

The unknown fault distance d_{L2} is obtained from Eqn. (29)

$$Re\{V_E\text{-}V_{se}\text{-}(Z_{L2}(1)\times I_E)\}$$
$$+ (d_{L2} \times Re(Z_{L2}(1)\times I_E)) - (R_{F2} \times Re(I_F)) = 0$$

(30)

$$Im\{V_E\text{-}V_{se}\text{-}(Z_{L2}(1)\times I_E)\}$$
$$+ (d_{L2} \times Im(Z_{L2}(1)\times I_E)) - (R_{F2} \times Im(I_F)) = 0$$

(31)

Fault point is obtained by evaluating Eqn. (30) and Eqn. (31),

$$d_{L2} = \frac{\begin{bmatrix}\{Re(V_E\text{-}(Z_{L2}(1)\times I_E))\}\times Im(I_F)\end{bmatrix} - \begin{bmatrix}\{Im(V_E\text{-}(Z_{L2}(1)\times I_e))\}\times Re(I_F)\end{bmatrix}}{\begin{bmatrix}\{Im(V_E\text{-}(Z_{L2}(1)\times I_E))\}\times Re(I_F)\end{bmatrix} - \begin{bmatrix}\{Re(V_E\text{-}(Z_{L2}(1)\times I_e))\}\times Im(I_F)\end{bmatrix}}$$

(32)

After the fault point d_{L2}, the unknown resistance (R_{F2}) is obtained by Eqn. (30).

$$R_{F2} = \frac{Re(V_E)-(1-d_{L2})\times Re(Z_{L2}(1)\times I_E)}{Re(I_F)}$$

(33)

At the relay location, *V* and *I* of all phases have been evaluated. And the symmetrical elements of the *V* and *I* have been assessed by using the SST algorithm.

4. Results and Simulation Study

4.1. Impedance trajectory and results

The system studied (Figure1) consists of two-line Sections: Section 1 provide from bus A1 to Bus E, in which section C is the fault bus section. Section 2 provides from bus E to Bus B1, in which section D is the fault bus section. A UPFC, rated with 100 MVA, is installed at the bus E i.e., at the mid-point of the system. The 500 kV, 300 km, the line network is supplied with 2 sources such as E_A and E_B of 1500 MVA, 500 kV, and with the angle, difference δ = 40° from both ends. For the modelling of transmission line sections, the distributed parameters line model is used. For + sequence component of Z_L is 0.204 + j3.527 Ω/km, for - sequence component of Z_L is 0.204 + j3.527 Ω/km, and 0 sequence component of Z_L is 2.542 + j12.25 Ω/km. A 2, 48 pulse inverter based on IGBT VSC cantered UPFC connected by two 2500 *μF* DC capacitors (common for both). One of the inverters is linked in series SSSC, whereas the second inverter is shunting STATCOM. The Δ/Y shunt transformer, i.e. a primary to the secondary rating is 500/15 kV, and the Y/Y series transformer, i.e. a primary to the secondary rating is 15/22 kV, was used as the STATCOM and SSSC coupling transformers. STATCOM (represented by Z_{sh} and V_{sh}) is used to regulate the voltage by injecting shunt current of varying magnitude SSSC (represented by Z_{se} and V_{se}) is used for injection of a sinusoidal voltage of magnitude which can be varied along with angle to regulate the power in the system.

4.2. Conditions of the studied system

The study system has been seen in Figure1, which simulated to analyse the accuracy of the method presented and to gain adequate results for various conditions, various fault circumstances as well as fault types. Simulations have been obtained for various fault positions i.e. 5-90% of the line network and R_F =5-200 Ω. By changing the series voltage (V_{se}) between 0-10 percent of the voltage level and also the V_{se} phase angle of the between 0°-360°, various operational characteristics can be generated. The relay is installed on the A1 bus. A sampling rate, 3.84 kHz, 3-phase measured currents (I_1), & voltages (V_{A1}) are sampled. Simulation is conducted by MATLAB/Simulink software.

4.3. Impedance trajectories during fault showing UPFC impact

Considering previous studies, it is confirmed that the incorporating UPFC in the transmission system, apparent impedance is altered significantly before and after the occurrence of the fault.
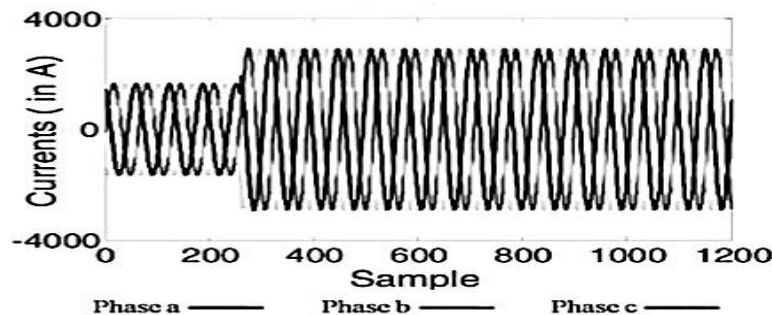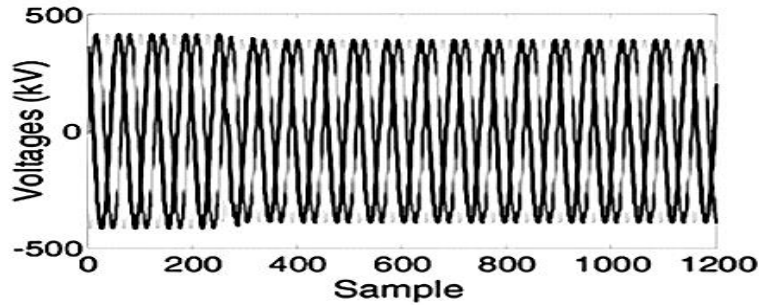
Figure 2. For ABC-G fault at D bus, 3-phase current and voltage signals in the time domain (before UPFC)
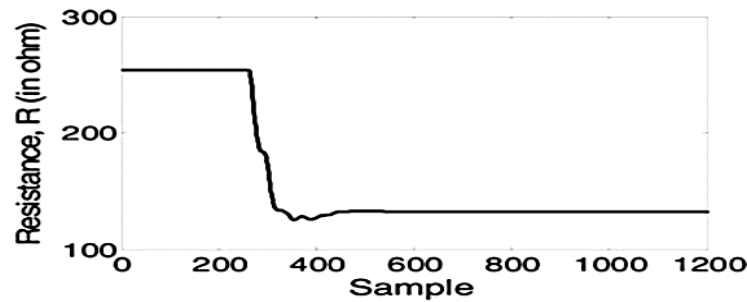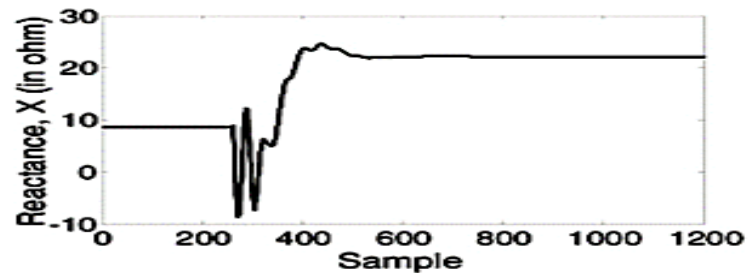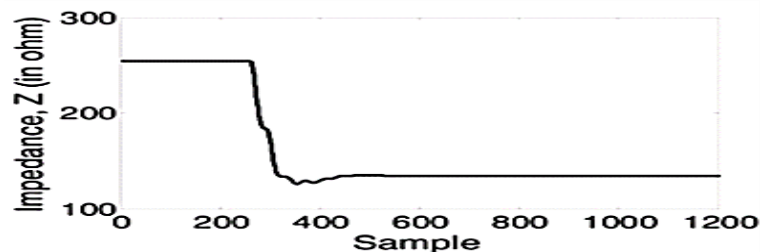

Figure 3. For fault ABC-G at bus D, apparent resistance trajectory (in absence of UPFC)

Thus, considering with and without UPFC, the influence of the same on the trajectories for bus D has been explored as sees. 3 phase a current and voltage signal (which is seen in Figure. 2) for ABC-G fault on bus D without UPFC (138 km). Results in Figure 3–6 shows ABC-G fault graphs on bus D with an R_F =30 before the UPFC. Figure. 3, Figure. 4 (a), and figure. 4 (b) illustrate the apparent R, X, and Z before the UPFC, respectively. For phases A, B as well as C for the same fault condition, the R-X paths are shown in Figure 6.

(a)

(b)

Figure 4. For fault ABC-G at bus D, (a) apparent reactance trajectory, (b) apparent impedance trajectory
(in absence of UPFC)

For the fault, ABC-G formed at bus D which is 138 km, for $R_F = 30\ \Omega$, three-phase voltage and current including UPFC (desired $P_{ref} = 7.9$ p.u. & the $Q_{ref} = -0.4$ p.u. is displayed in Figure 6. Figure 7 to 8 show the R_{app} and X_{app} respectively. The Z_{app} seen by the relay has been displayed in Figure 9. For the same distance and same fault, the R-X trajectory is shown in Figure 10.
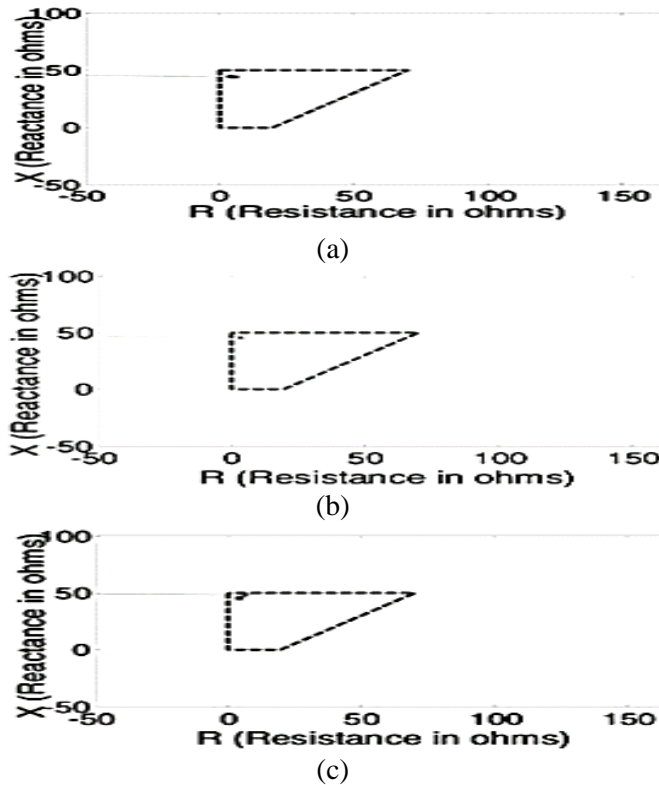

(a)

(b)

(c)

Figure 5. For fault ABC-G at D bus, apparent impedance trajectory (in absence of UPFC), Phase-A ((a)), Phase-B (b), Phase-C (c)

From the above-mentioned results, it is observed that suitable compensatory measures are needed to be taken to avoid significant deviations in the relay operation, due to the presence of UPFC (over-reaching/under-reaching).

5. Analytical Performance of Algorithm for Fault Location

Fault position of the fault occurring at bus C without UPFC is acquired as,

$$L_1 = (d_{L1} \times Z_{L1}(1)) \tag{36}$$

Fault location deviation (without UPFC) is given by,

$$Deviation(\%) = (L_1 - L_{FP1} / L_{Total} \times 100) \tag{37}$$

Where, L_C - Real fault distance to fault position C
L_{Total} -the entire line length (from A1 to B1 bus).
Also, for fault occurring after UPFC (D), fault location in km is given by,

$$L_2 = ((1 - d_{L2}) \times Z_{L2}(1)) + Z_{L1}(1) \tag{38}$$

Fault location deviation after UPFC has been specified,

$$\% Error = (L_2 - L_{FP2}) / L_{Total} \times 100 \tag{39}$$

Where, L_D - Real fault distance to fault position D
Results of fault point for L-G faults (C-G fault) without the UPFC are shown in Figure 11. For the system conditions stated as fault distance of 30% for $\alpha = 50°$ and $\delta = 40°$. The R_F is set to be $R_{F1} = 3\ \Omega$ & 200 Ω, V_{se} of the UPFC is 0 to 10% with a phase angle of 180°. $P_{ref} = 7.9$ p. u. and $Q_{ref} = -0.4$ p.u. Figure 11 depicts the percentage location deviation is 0.87% for 3 Ω R_F and location deviation is

4.71% for $R_F = 200$ Ω. The fault locations of balanced LLL-G fault before the UPFC are shown in Figure 12 for system conditions stated as fault distance of 10% with δ = 40° and α = 30°. The $R_{F2} = 3$ Ω to 200 Ω, $P_{ref} = 7.9$ p. u. and $Q_{ref} = -0.4$ p.u. For the $R_F = 3$Ω, the deviation in estimating fault position has been low i.e. 0.61% and for high R_{F2} is very high i.e. 200 Ω, estimating fault location is high (4.86%). Figure 13 depicts the fault position outcomes for A-G fault for system conditions stated as δ = 40° and α = 30°. The R_{F2} is 3 Ω to 150 Ω at a fault distance of 84%. The P_{ref} is 7.9 p. u. as well as Q_{ref} is −0.4 p.u. respectively. For the R_F of 3 Ω, the deviation in estimating fault position is low (0.30%) and for high (R_{F2}) is higher (150 Ω), estimating fault position is high (4.86%).

Figure 14 represents the fault position results for AB-G fault, for the system conditions as fault point of 66% with δ = 40° and α = 90°. The R_F is set to be $R_F = 3$ to 200Ω. The active and reactive power is $P_{ref} = 7.9$ p. u. and $Q_{ref} = -0.4$ p. u. respectively. It is observed that the fault point deviation = 0.71% w.r.t. $R_F = 3$Ω and the fault point deviation 4.29%. When $R_{F2} = 200$ Ω for L-L (A-C phase) fault occurred at the fault location D w.r.t. UPFC the results are mentioned in Figure 15, for the system conditions stated as fault distance of 55% for α = 30° and δ = 40°. The R_F is set to be $R_{F2} = 20$ Ω & 200 Ω, and the V_{se} of the UPFC is 0 to 10% having a phase angle of 180°.
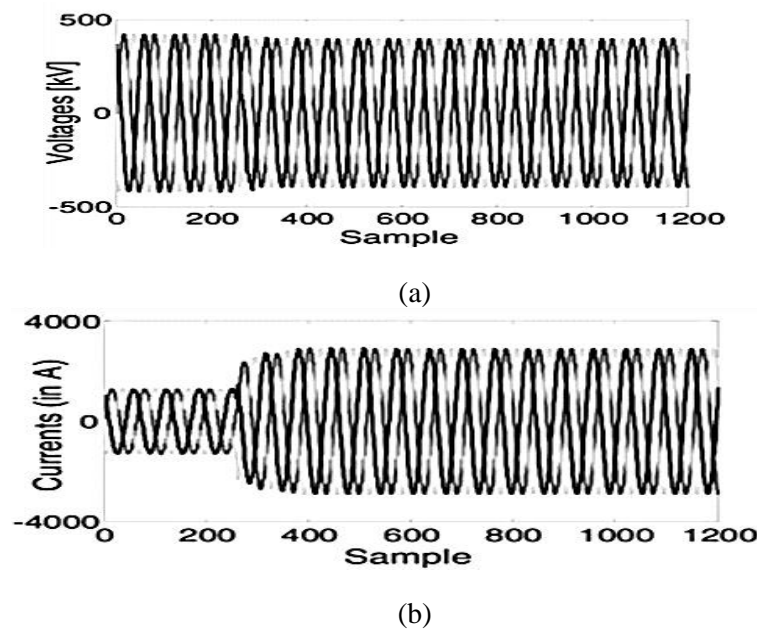

(a)

(b)

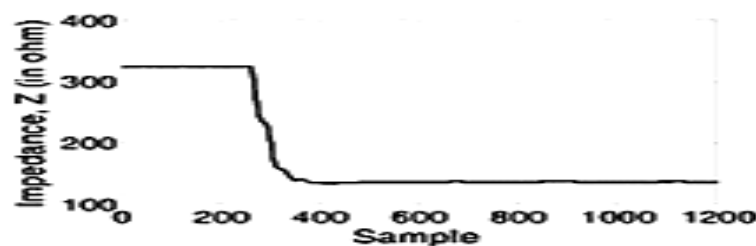**Figure 6.** Time domain signals after UPFC (a) three phase voltages, (b) three phase currents

Figure 7. Apparent impedance representation besides ABC-G fault on the D bus after UPFC

From Figure 15, it is clear that at $R_F = 20$ Ω, the deviation in locating fault changes from 0.32 to 2.45%, and for $R_F = 200$ Ω, the deviation percentage changes from 0.45 to 2.97%, while other system operating conditions remained constant.
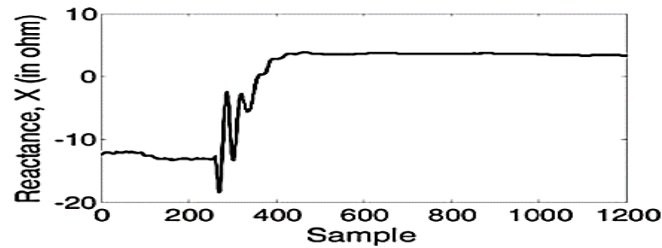
Figure 8. Apparent reactance representation besides ABC-G fault on the D bus after UPFC

The simulation study has shown that there are variations of different systems components such as an injected voltage of UPFC, phase angle as well as impedance of fault which cause fault location inaccuracies to alter.
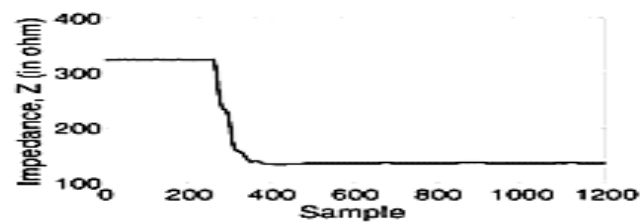

Figure 9. Apparent impedance representation besides ABC-G fault on the D bus after UPFC
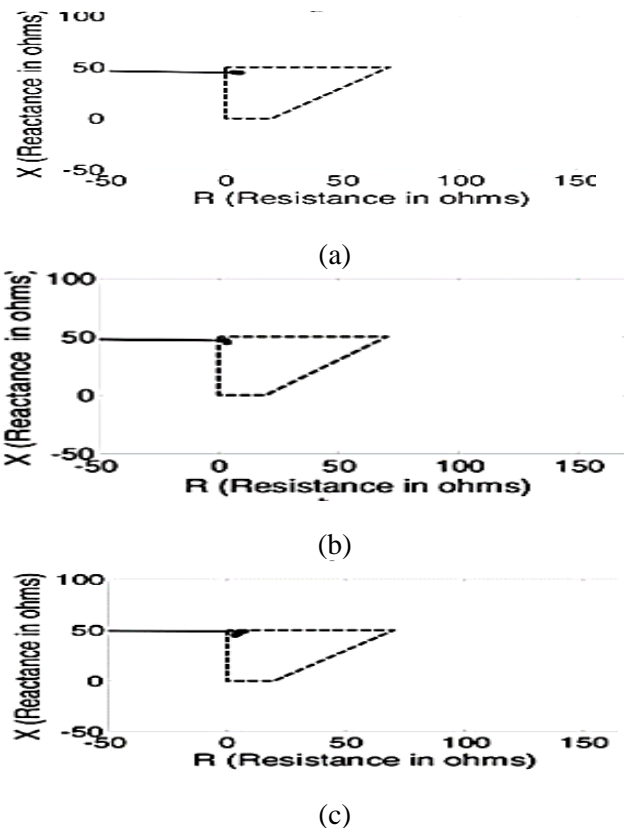

(a)

(b)

(c)

Figure 10. Apparent impedance trajectory besides ABC-G fault on the D bus with UPFC (a) Phase-A, (b) Phase-B, (c) Phase-C

The influence of the controller on the distance relay also has a dependence on the position at which the device is installed in the line and the system condition. Results of fault point for B-G fault with the

UPFC located at different locations are shown in Figure 16 for the system conditions stated as α is 90° and δ is 40°. The R_F is set to 3 Ω and 200 Ω (R_{F1}). The series injected voltage of UPFC is 10% with a phase angle of 360°. Figure 16 depicts the results of fault location for the various faults showcasing that deviation in locating faults, remains are within the acceptable limits, irrespective of UPFC location. For higher R_F= 200 Ω, the developed algorithm is validated. Further, observed the small change in the fundamental component (0.5 Hz) results in a fault location deviation of 0.2%, which is very low & suitable for determining fault point.
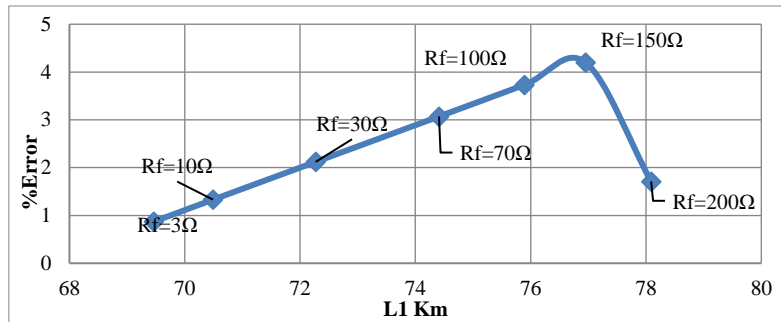

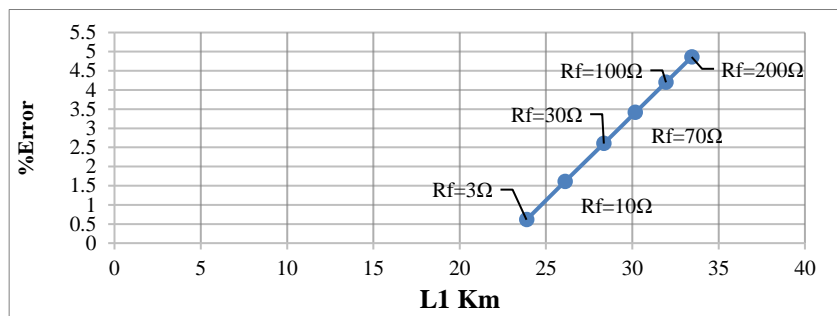**Figure 11.** Results of locating fault for fault C-G at 30% of line, L_{FP1}=67.5 km

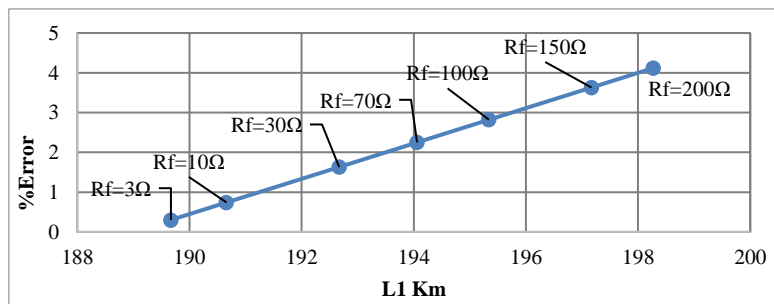**Figure 12.** Results of locating fault for fault ABC-G at 10% of line, L_{FP1}=22 km

Figure 13. Results of locating fault for fault A-G at 84% of line, L_{FP1}=189 km
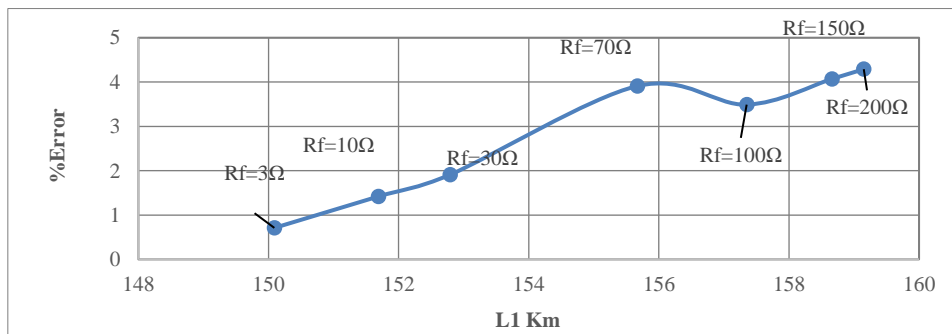
Figure 14. Results of locating fault for fault AB-G at 66% of line, L_{FP1}=148.2 Km
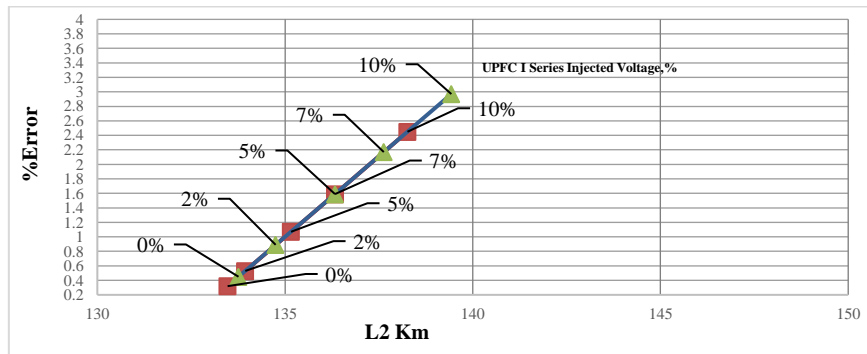

Figure 15. Results of locating fault for fault ABC-G at 55% of line, L_{FP1}=123.7 km
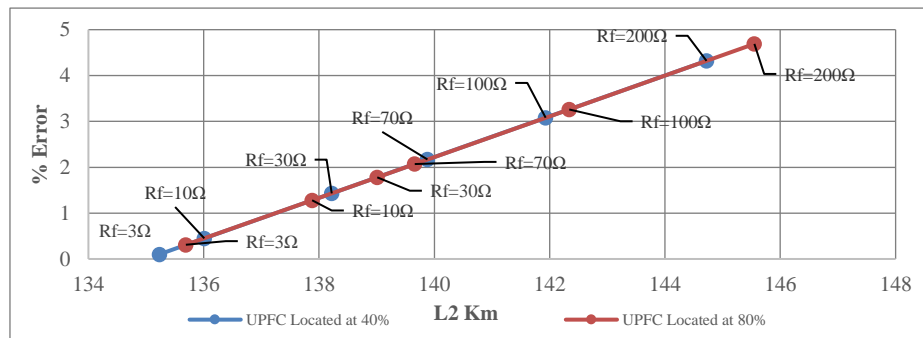

Figure 16. Results of locating fault for fault B-G at 60% of the line for different UPFC position, L_{FP1}=123.7 km

5. Conclusion

A method for locating various faults on the UPFC-compensated transmission system using a sparse ST is presented. Sparse ST uses formulated S-matrix sparsity, which reduces the burden of calculation by an excellent frequency-scaling technique. To obtain the fundamental phasors of current and voltage including the phase angle, the SST algorithm has been used to introduce a new concept of phase correction (a prerequisite for fault location estimation). To study the impact of various UPFC voltage, fault resistance, as well as phase angle values on a transmission system fault location of the system parameters, the results have been shown. It's also confirmed from simulation studies that its estimation of fault location is more accurate for low impedance faults than for high impedance faults. For faster operation and appropriate fault location, Sparse ST has been formed to protect the UPFC-integrated electricity grid.

References

1. Hingorani N. G. & Gyugyi L. (2000). *Understanding FACTS Concepts and Technology of Flexible AC Transmission Systems*. New York: IEEE Press.
2. Zhou X, Wang H, Aggarwal R. K, Beaumont P. (2006). Performance evaluation of a distance relay as applied to a transmission system with UPFC. *IEEE Trans. Power Deliv.*, *21*(3), 1137–1147
3. Albasri F. A, SidhuT. S. and Varma R. K. (2007). Performance comparison of distance protection schemes for shunt-FACTS compensated transmission lines. *IEEE Trans. Power Deliv.* *22*(4), 2116–2125.
4. Pandey S. P. and Tripathy M. (2010). Impact of UPFC on distance relay: *A case study, Int. Conf. on Power, Control and Embedded Systems, Allahabad*. 1-4.

5. Deshmukh N, Bedi A. S. and Patne N. R. (2016). Analysis of distance protection performance for line employing UPFC. *IEEE 1ˢᵗ Int. Conf. on Power Electronics, Intelligent Control and Energy Systems (ICPEICES), Delhi,* 1-4.
6. Moravej Z, Pazoki M. and Khederzadeh M. (2014). Impact of UPFC on Power Swing Characteristic and Distance Relay Behavior. *IEEE Trans. on Power Delivery*, 29(1), 261-268.
7. Khodaparast J, Khederzadeh M, Faria da Silva F. and Bak C. L. (2016). Variation of UPFC controllable parameters during power swing and their impacts on distance relay. *IET Generation, Transmission & Distribution*, 11(7), 1735-1744.
8. Zhang L, Zhou B, Li P, Yuan Y, Xu J. and Kong X. (2019). Impact Evaluation for Distance Protection of Southern Suzhou 500kV UPFC. *14th IEEE Conf. on Industrial Electronics and Applications (ICIEA), Xi'an, China*, 293-298.
9. Khade Priyanka & Patil V. S. (2019). Mal-Operation of Mho Relay in Transmission Line due to Presence of TCSC. *Int. Journal of Recent Tech., and Engineering (IJRTE)*, 8(3), 2579-2586.
10. Gaidhani T. S. & Kale A. K. (2019). VSC-HVDC Bipolar Grid Based on Novel Distance Protection Scheme. *Int. Journal of Recent Tech., and Engineering (IJRTE)*, 8(3), 1527-1532.
11. Osman A. H. & Malik O. P. (2004). Transmission line distance protection based on wavelet transform. *IEEE Trans. on Power Delivery*, 19(2), 515-523.
12. Kirubadevi S. and Sutha S. (2017). Wavelet based transmission line fault identification and classification. *Int. Conf. on Computation of Power, Energy Information and Communication (ICCPEIC), Melmaruvathur*, 737-741.
13. Ray P, Mishra D. P. and Mohaptra S. (2016). Fault classification of a transmission line using wavelet transform & fuzzy logic. *IEEE 1st Int. Conf. on Power Electronics, Intelligent Control and Energy Systems (ICPEICES), Delhi,* 1-6.
14. Stockwell R. G, Mansinha L. & Lowe R. P. (1996). Localization of the complex spectrum: The S transform. *IEEE Trans. on Signal Processing,* 44(4), 998-1001.
15. Dash P. K, Samantaray S. R. & Panda G. (2005). Fault analysis of advanced series compensated line using S-transform and pattern recognition approach. *Int. Power Engineering Conf., Singapore,* 1-484.
16. Thakre M. P. & Kale Vijay S. (2016). An Adaptive Approach for Three Zone Operation of Digital Distance Relay with Static Var Compensator using PMU. *Electrical Power & Energy Systems,* 77, 327-336.
17. Ahmadimanesh A. and Shahrtash S. M. (2013) Transient-Based Fault-Location Method for Multiterminal Lines Employing S-Transform. *IEEE Transactions on Power Delivery,* 28(3), 1373-1380.
18. Krishnanand, K.R, Dash, P.K. (2013). A new real-time fast discrete S-transform for cross-differential protection of shunt-compensated power systems. *IEEE Trans. Power Deliv,* 28(1), 402–410.
19. Das, Sahasransu, Joymala M, & Dash P. K. (2015). Distance protection of shunt compensated transmission line using a sparse S-transform, *IET Generation Transmission & Distribution.*
20. Tripathy L. N, Samantaray S. R. & Dash P. K. (2015). Location of fault on UPFC based transmission lines using sparse S-Transform. *IEEE Power, Communication and Info. Technology Conf. (PCITC), Bhubaneswar,* 167-172.
21. Biswas S. and Nayak P. K. (2020). A Fault Detection and Classification Scheme for Unified Power Flow Controller Compensated Transmission Lines Connecting Wind Farms. *IEEE Systems Journal.*
22. Thakre M. P. & Kale V. S. (2015). Study and Mitigation of Subsynchronous Oscillations with SSC Based SSSC. *Journal of Power and Energy Engineering*, 3(9), 33-43.
23. Raju D. Koteswara & Umre B. S. (2016). Fractional-Order PI Based UPFC Damping Controller to Mitigate Subsynchronous Resonance. *SpringerPlus*, 5, 1-20.